ISSN 2706-655X Vol. 7, Issue 3: 1-8, DOI: 10.25236/IJFET.2025.070301

Maximum Power Improvement Active Disturbance Rejection Control for Wind Turbines

Jing Li[1,a,*], Hao Li[1,b]

[1]*School of Electrical Engineering and Automation, Henan Polytechnic University, Jiaozuo, China*
[a]*891298810@qq.com*, [b]*lh1739246516@outlook.com*
**Corresponding author*

Abstract: *Aiming at the problems of linear active disturbance rejection control (LADRC) in the permanent magnet direct - drive wind power generation system, such as non-full decoupling between dynamic and immunity performance and poor observation accuracy, an improved active disturbance rejection control method with a compensation function observer (CFO - LADRC) is proposed. A speed controller with CFO - LADRC is designed based on maximum power tracking with the optimal tip speed ratio, resolving the performance trade-off and improving immunity. Frequency domain analysis shows that it's better than conventional LADRC. Simulation comparison reveals that it can effectively enhance the anti - disturbance ability while retaining the advantages of the conventional method.*

Keywords: *Wind Power Generation; Permanent Magnet Synchronous Generator; Maximum Power Tracking Control; Compensation Function Observer; Active Disturbance Rejection Control*

1. Introduction

Wind energy, a renewable and eco-friendly new energy source, has drawn global attention. However, wind energy signals are random, intermittent, abrupt and unstable. Thus, researching maximum power point tracking (MPPT) control for wind power systems is of great practical significance to fully use wind energy, mitigate wind speed fluctuation impacts and enhance system robustness[1]. Currently, wind power control technology applications are diversified. Domestic and foreign scholars focus more on wind power system control technology research and have achieved good results in existing and advanced control methods like PID control[2], adaptive control[3], sliding mode control[4].

ADRC can regard the internal and external disturbances and uncertainties of the controlled object as the total disturbance, which is then estimated and compensated for by an extended state observer[5]. Reference [6] introduces the anti-jitter factor function and proposes an improved ADRC. Reference [7] proposes an improved nonlinear ADRC, which constructs the observer using a smooth nonlinear function to realize the maximum power tracking. Reference [8] applies LADRC to speed loops, aiming to achieve maximum power output and improve system robustness and immunity. Reference [9] proposes a composite control scheme combining LADRC and position sensor-less technology, which significantly improves the control performance, immunity, and observation accuracy compared with the ordinary LADRC. Reference [10] designs a model self-correcting composite active disturbance rejection control. The speed loop adopts an ADRC that can switch between nonlinearity and linearity to improve immunity and response speed. Reference [11] proposes a hybrid control method combining fuzzy control and LADRC, which uses fuzzy control to dynamically adjust the parameters to enhance immunity and robustness.

However, the above LADRC controller is unable to fully decouple the system dynamics and disturbance resistance performance, and a balance needs to be struck between the two in practical applications, which increases the difficulty of controller parameter adjustment[12]. In this paper, the compensation function observer (CFO) is introduced into the LADRC, and a CFO-based LADRC method is proposed. This method is designed to observe parameters of the wind turbine, including the collection of relevant parameters, internal and external perturbations. Then, the observation results are fed back to the LSEF for perturbation compensation, which improves the anti-disturbance performance of the wind power system. The method takes into account the fast dynamic response and good anti-disturbance performance, solves the trade-off between the two, and further enhances the anti-disturbance capability.

ISSN 2706-655X Vol. 7, Issue 3: 1-8, DOI: 10.25236/IJFET.2025.070301

2. Direct-Drive Wind Power System Model

The structure of the direct-drive permanent magnet synchronous wind power generation system is shown in Fig. 1. It is mainly composed of a wind turbine, a synchronous generator, a converter, and a transformer.

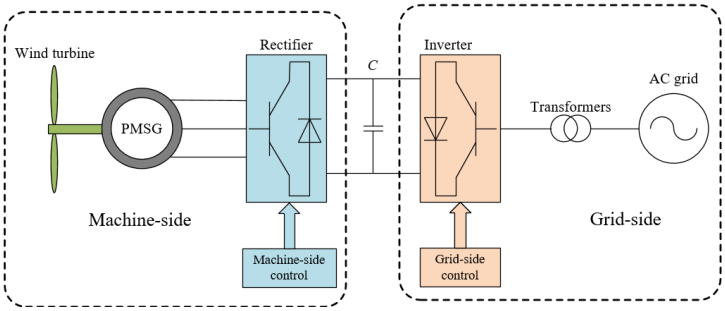

Fig. 1 Basic structure of direct-drive permanent magnet synchronous wind power generation system

2.1 Wind Turbine Modeling

The wind power generation system captures wind energy through the wind turbine blades and converts it into mechanical energy, which is then transferred with torque to the permanent magnet synchronous generator (PMSG) to be converted into electrical energy. According to Betz theory, the wind turbine output power P_w is expressed as:

$$P_w = \frac{1}{2}\rho\pi R^2 v^3 C_p(\lambda,\beta) \tag{1}$$

where ρ is the air density; R is the radius of the turbine blade; v is the wind speed; $C_p(\lambda,\beta)$ is the wind energy utilization coefficient; β is the pitch angle; and λ is the blade tip speed ratio.

$$\lambda = \frac{\omega_m R}{v} \tag{2}$$

where ω_m is the angular velocity of the wind turbine.

The wind energy utilization coefficient C_p serves as a function of the blade tip speed ratio λ and the pitch angle β.

$$C_p(\lambda,\beta) = 0.5176\left(\frac{116}{\lambda_i} - 0.4\beta - 5\right)e^{-\frac{21}{\lambda_i}} + 0.0068\lambda \tag{3}$$

$$\frac{1}{\lambda_i} = \frac{1}{\lambda + 0.08\beta} - \frac{0.035}{\beta^3 + 1} \tag{4}$$

The function curve of $C_p(\lambda,\beta)$ is shown in Fig. 2.

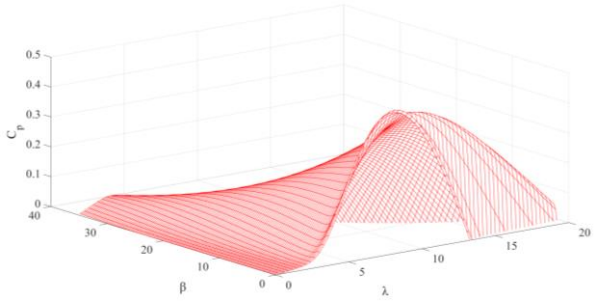

Fig. 2 Wind energy coefficient curve

At a fixed pitch angle, there is an optimal tip speed ratio corresponding to the maximum wind energy utilization coefficient, and in this case the maximum output power can be obtained. Adjusting the blade tip speed ratio can enable the wind turbine to realize the maximum wind energy utilization under different working conditions and achieve the maximum power tracking. It can be seen that maximum power tracking is essentially tracking the generator's rotational speed.

ISSN 2706-655X Vol. 7, Issue 3: 1-8, DOI: 10.25236/IJFET.2025.070301

2.2 Permanent Magnet Synchronous Generator Model

The mathematical model of PMSG in $d-q$ coordinate system can be described as follows:

$$\begin{cases} u_d = L_d \dfrac{di_d}{dt} + R_s i_d - L_q n_p \omega_g i_q \\ u_q = L_q \dfrac{di_q}{dt} + R_s i_q + L_d n_p w_g i_d + n_p \omega_g \psi_f \end{cases} \tag{5}$$

where $u_d,\ u_q,\ i_d,\ i_q,\ L_d,\ L_q$ are the voltage, current, and inductance components of the motor in the d-axis and q-axis, respectively; R_s is the stator resistance; ψ_f is the magnetic chain of the permanent magnets; n_p is the number of pole pairs of the motor rotor; and ω_g is the mechanical angular velocity of the generator rotor.

With the $i_d^* = 0$ magnetic field-oriented vector control technique, it is possible to obtain the electromagnetic torque of the generator as follows:

$$T_e = \frac{3}{2} n_p \psi_f i_q = k_t i_q \tag{6}$$

The direct-drive permanent magnet synchronous wind power system does not require a variable speed gearbox, so that the angular velocity of the generator rotor is the same as that of the wind turbine, i.e., $\omega_g = \omega_m$. Therefore, the mathematical model of the wind power drive train can be expressed as follows:

$$\frac{\mathrm{d}\omega_m}{\mathrm{dt}} = \frac{1}{\mathrm{J}}(T_L - T_e - B\omega_m) \tag{7}$$

where J is the rotational inertia; T_L is wind turbine output torque; B is the viscous friction factor.

3 Design of A Rotational Speed Loop LADRC with Compensating Function Observer

The ADRC can consider the internal and external perturbations and uncertainties of the controlled object as a new state, and then use LESO to estimate the state, and then enhance the system dynamics performance through compensation.

From Eq. (6) and Eq. (7), the generator speed output can be simplified as.

$$\dot{\omega}_m = \frac{1}{J}(T_L - B_m\omega_m - k_t i_q) \tag{8}$$

Equation (8) can be expressed as:

$$\dot{\omega}_m = f + b_0 i_q \tag{9}$$

where f is the total perturbation of the system, $f = \frac{1}{\mathrm{J}}(T_L - B_m\omega_m);\ b_0 = -\frac{k_t}{J}$.

The error between the observer's observed and actual values of the system state variables and total perturbations is a key factor affecting the quality of ADRC control. The smaller the error, the better the system robustness and immunity to perturbation. Taking $x_1 = \omega_m,\ x_2 = f,\ u = i_q$, the system state equation can be described by Eq. (10).

$$\begin{cases} \dot{x}_1 = x_2 + b_0 u \\ \dot{x}_2 = \dot{f} \\ y = x_1 \end{cases} \tag{10}$$

LESO can be designed as follows:

$$\begin{cases} \dot{z}_1 = \hat{f} + \beta_1(y - z_1) + b_0 u \\ \dot{\hat{f}} = \beta_2(y - z_1) \end{cases} \tag{11}$$

where z_1 is the estimate of x_1; $\hat{f}$ is the estimate of f; β_1 and β_2 are the observer gains.

Conventional LESO has insufficient ability to observe uncertain nonlinear time-varying perturbations and does not include $\beta_1(y - z_1)$ as part of the perturbation observation. This approach avoids output oscillations, but the total perturbation cannot be completely eliminated when tracking the time-varying

ISSN 2706-655X Vol. 7, Issue 3: 1-8, DOI: 10.25236/IJFET.2025.070301

reference signal.

In order to accurately observe the uncertain nonlinear time-varying perturbations, a compensating perturbation observation term $\tilde{f}$ is introduced in the observer design. The following observer can be designed to observe ω_m and f.

$$\begin{cases} \dot{z}_1 = \tilde{f} + \beta_1(y - z_1) + b_0 u \\ \hat{f} = \tilde{f} + \beta_2(y - z_1) \end{cases} \tag{12}$$

The observation error can be calculated by Eq. (10) and Eq. (12).

$$\dot{e} = f - \tilde{f} - \beta_1 e \tag{13}$$

where $e = y - z_1$. The total disturbance estimation error directly affects the observation error and volatility of ω_m. In order to minimize the observation error and volatility, $\tilde{f}$ needs to observe f as accurately as possible. The link between them can be constructed with the help of a low-pass filter, which is expressed as follows:

$$\tilde{f} = \frac{\lambda}{s + \lambda} \hat{f} \tag{14}$$

Associating Eq. (12) and Eq. (14), the improved observer can be simplified as:

$$\begin{cases} \dot{z}_1 = z_2 + \beta_1(y - z_1) + b_0 u \\ \dot{z}_2 = \lambda\beta_2(y - z_1) \\ f_w = z_2 + \beta_1(y - z_1) \end{cases} \tag{15}$$

where $z_2 = \tilde{f}$ is the compensation function and f_w is the compensated perturbation estimate.

Configuring the poles to $-\omega_o$ using the bandwidth method yields the following parameters.

$$\beta_1 = 2\omega_o, \beta_2 = \omega_o, \lambda = \omega_o \tag{16}$$

LSEF can be designed to:

$$u = \frac{\omega_c(\omega_{ref} - z_1) - f_w}{b_0} \tag{17}$$

where ω_c is the controller bandwidth and ω_{ref} is the desired output.

The block diagram of the maximum power control of the wind power system is shown in Fig. 3.

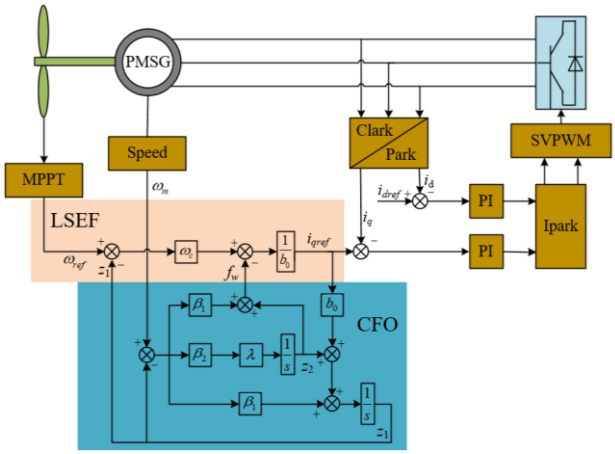

Fig. 3 Block diagram of maximum power control of wind power system

4. Frequency Domain Analysis

4.1 Analysis of Decoupling Characteristics

From Eq. (15) and Eq. (16), the transfer functions of z_1, z_2, and f_w are:

ISSN 2706-655X Vol. 7, Issue 3: 1-8, DOI: 10.25236/IJFET.2025.070301

$$\begin{cases} z_1 = \dfrac{2\omega_o s + \omega_o^2}{(s+\omega_o)^2} y + \dfrac{b_0 s}{(s+\omega_o)^2} u \\ z_2 = \dfrac{\omega_o^2 s}{(s+\omega_o)^2} y - \dfrac{b_0 \omega_o^2}{(s+\omega_o)^2} u \\ f_w = \dfrac{2\omega_o s^2 + \omega_o^2 s}{(s+\omega_o)^2} y - \dfrac{2b_0\omega_o s + b_0\omega_o^2}{(s+\omega_o)^2} u \end{cases} \tag{18}$$

It is possible to derive the transfer function of the control quantity u as follows:

$$\begin{cases} u = \dfrac{1}{b_0} C(s)[\omega_c r - H(s) y] \\ C(s) = \dfrac{(s+\omega_o)^2}{s(s+\omega_c)} \\ H(s) = \dfrac{\omega_o(s+\omega_c)(2s+\omega_o)}{(s+\omega_o)^2} \end{cases} \tag{19}$$

To simplify the analysis process, it is assumed that the response of the current controller in the PMSG system is fast enough, so that the velocity closed-loop system can be equivalent to the structure shown in Fig. 4.

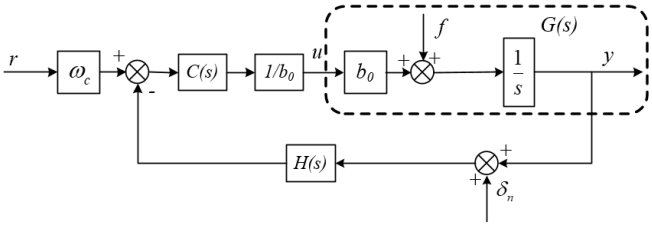

Fig. 4 Closed-loop system control block diagram

Thus, the output quantity y can be expressed as:

$$\begin{cases} y = G_r(s) r + G_f(s) f + G_n \delta_n \\ G_{\mathrm{r}}(s) = \dfrac{y}{r} = \dfrac{\omega_c}{s+\omega_c} \\ G_f(s) = \dfrac{y}{f} = \dfrac{s}{(s+\omega_o)^2} \\ G_n(s) = \dfrac{y}{\delta_n} = -\dfrac{2\omega_o s + \omega_o^2}{(s+\omega_o)^2} \end{cases} \tag{20}$$

From Eq. (20), $G_{\mathrm{r}}(s)$ is only related to the controller gain ω_c, and $G_f(s)$ depends only on the observer bandwidth ω_o, independent of ω_c. This indicates that the dynamic performance is determined by ω_c, independent of the observer's bandwidth, and the immunity performance depends on ω_o, independent of ω_c. Therefore, the LESF and CFO of the proposed improved LADRC can be independently tuned. Overall, the CFO-LADRC is a two-degree-of-freedom controller that can realize the complete decoupling of dynamic and immunity performance.

4.2 Observer Performance Analysis

To demonstrate the enhancement in the immunity performance of CFO-LADRC, a comparison was made between the immunity of CFO and that of LESO.

From Eq. (20), the transfer function of CFO immunity performance is:

$$G_f(s) = \frac{y}{f} = \frac{s}{(s+\omega_o)^2} \tag{21}$$

Similarly, the transfer function of the LESO immunity performance is:

$$G_f'(s) = \frac{s^2 + (2\omega_o + \omega_c)s}{(s+\omega_c)(s+\omega_o)^2} \tag{22}$$

Under the condition of selecting the same observer bandwidth ω_o, the results of the comparison of

ISSN 2706-655X Vol. 7, Issue 3: 1-8, DOI: 10.25236/IJFET.2025.070301

the immunity performance of CFO and LESO are shown in Fig. 5. CFO and LESO have similar ability in suppressing high-frequency interference. However, CFO is better than LESO in suppressing low and medium frequency interference. Overall, CFO realizes the complete decoupling of dynamic performance and anti-interference performance, which improves the anti-interference capability.

Setting $e_f = f - f_w$, the CFO transfer function between the disturbance estimation error e_f and the total disturbance f is obtained as:

$$G_{ef}(s) = \frac{s^2}{(s+\omega_o)^2} \tag{23}$$

Using the same approach, it is possible to derive the LESO transfer function between the perturbation estimation error e_f and the total perturbation f as:

$$G'_{ef}(s) = \frac{s^2 + 2\omega_o s}{(s+\omega_o)^2} \tag{24}$$

To ensure the fairness of the comparison, the same bandwidth ω_o is chosen for both. The perturbation estimation capabilities of CFO and LESO are shown in Fig. 6. Compared with LESO, CFO is able to observe low-frequency perturbations more accurately, and it also realizes the observation of mid-frequency and high-frequency perturbations without steady state errors. Therefore, CFO has more excellent disturbance estimation capability.

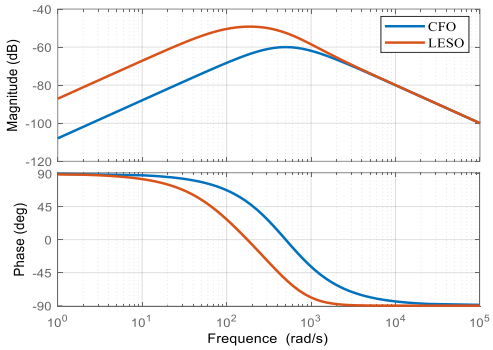

Fig. 5 Comparison of the immunity performance of the two observers

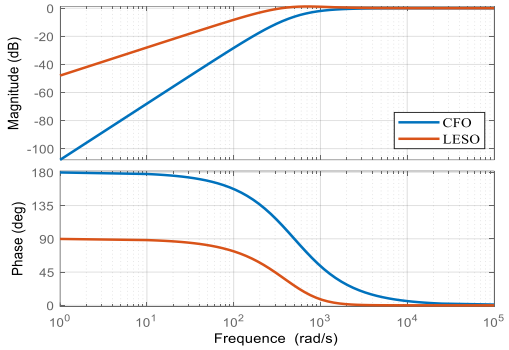

Fig. 6 Comparison of the perturbation estimation capabilities of the two observers

5. System Simulation and Analysis

In order to verify the effectiveness of the CFO-LADRC controller proposed in this paper, a mathematical model of the wind power system is constructed in the MATLAB/Simulink environment. Then, the natural wind field is decomposed into three types of wind fields, namely gust wind, gradient wind, and turbulent wind and the speed tracking under these three different wind conditions is observed, compared, and analyzed with that of the PI control and LADRC.

5.1 Gust Wind Simulation Analysis

Gusts are used to describe the nature of sudden changes in wind speed, with the gust starting at 0.1 s, having a period of 0.3 s, and a peak of 9 m/s. Fig. 7 shows the comparative curves of the system's speed tracking capability and wind energy utilization coefficients under the effect of gusts.

From Fig. 7, it can be seen that after the wind power generation system is started, there is an overshoot of the rotational speed in the startup phase of the PI control, and there is no obvious overshoot of the rotational speed in the startup of the LADRC control and the CFO-LADRC control proposed in this paper. The time to reach equilibrium varies among the three control methods, with the PI control taking 0.1 s, the LADRC control taking 0.04 s, and the CFO-LADRC control taking only 0.01 s. In terms of wind energy utilization, the CFO-LADRC control enables the system to reach the maximum wind energy utilization efficiency faster and stabilizes it at 48%. The controller proposed in this paper tracks the optimal speed of the system with a faster response and higher accuracy and has good adaptability and effectiveness in the face of complex external disturbances.

ISSN 2706-655X Vol. 7, Issue 3: 1-8, DOI: 10.25236/IJFET.2025.070301

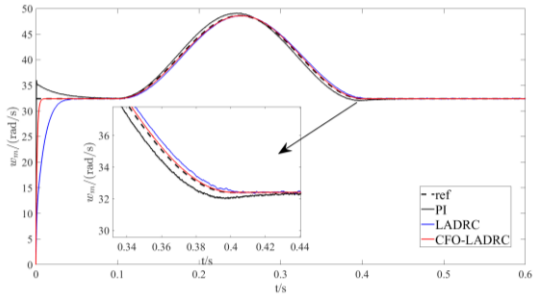

(a) Comparison curve of system speed tracking capability

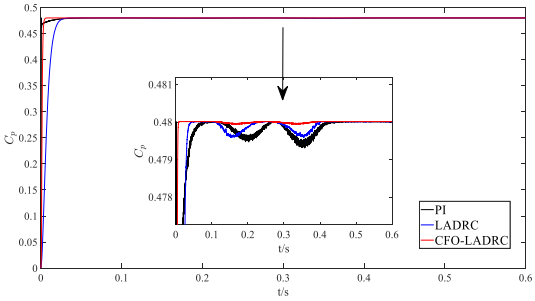

(b) Wind energy utilization factor comparison curve

Fig. 7 Comparison of different control strategies under gust wind action

5.2 Gradient Wind Simulation Analysis

The asymptotic wind describes the gradual change of wind speed characteristics. It starts at 0.2 s and ends at 0.4 s, peaking at 8 m/s and lasting for 0.1 s. Fig. 8 shows the comparison curves of the system's speed tracking ability and wind energy utilization coefficient under the influence of the asymptotic wind.

In the stage of slow wind speed change, compared with other control algorithms, the CFO-LADRC method adopted in this paper has better performance and higher control accuracy of the optimal speed. When the wind speed suddenly decreases and the working conditions change, the method responds faster and can react to the sudden change of wind speed in a very short time, and the whole control process can be realized without overshooting, which guarantees the stable and precise operation of the system.

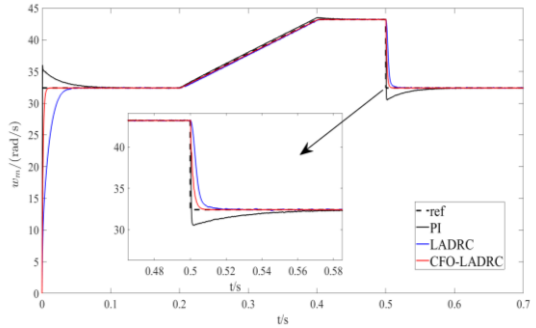

(a) Comparison curve of system speed tracking capability

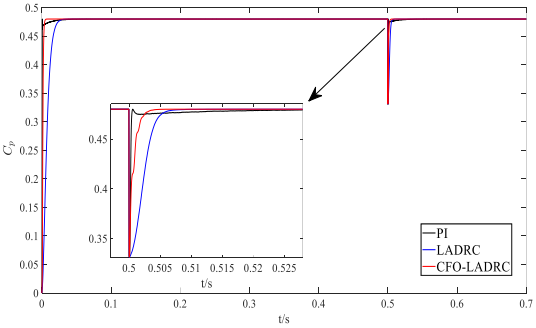

(b) Wind energy utilization factor comparison curve

Fig. 8 Comparison of different control strategies under the effect of gradient wind action

5.3 Stochastic Wind Simulation Analysis

Random wind can be used to describe the randomness of wind speed at the height of the impeller. In this paper, random noise wind is used to simulate the random wind. Fig. 9 shows the curve of the system speed tracking capability versus the wind energy utilization factor under the effect of random wind.

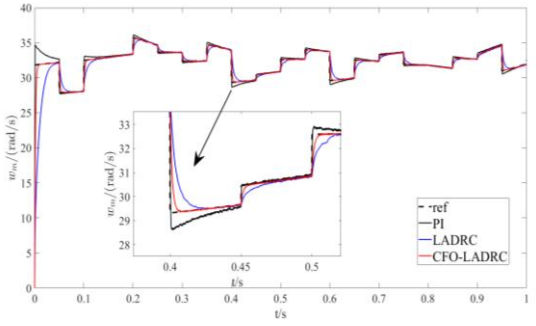

(a) Comparison curve of system speed tracking capability

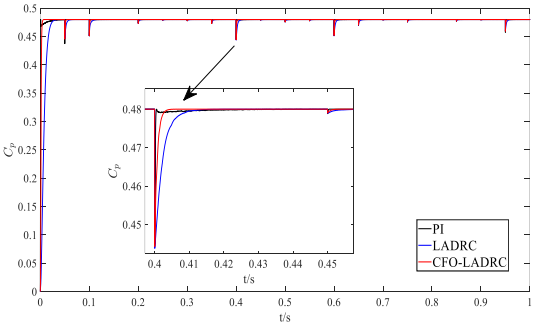

(b) Wind energy utilization factor comparison curve

Fig. 9 Comparison of different control strategies under random wind action

ISSN 2706-655X Vol. 7, Issue 3: 1-8, DOI: 10.25236/IJFET.2025.070301

Under the complex working condition of random wind speed change, the control effect of different control algorithms varies significantly: the PI control produces a large overshooting phenomenon when the wind speed changes; the LADRC has a good performance in speed tracking without overshooting problem, but the response time is longer. The CFO-LADRC control algorithm used in this paper not only has a faster response time in tracking and controlling the optimal rotational speed, which can quickly detect the wind speed changes and adjust the system state in time, but also has a higher control accuracy, which ensures that the system always operates stably and accurately.

6. Conclusions

In this paper, based on the research on the maximum power tracking of direct-drive permanent magnet synchronous wind power generation system, a CFO-LADRC control method is proposed for the PMSG system with LADRC speed controller, which has the problems of poor disturbance immunity and incomplete decoupling of dynamic performance and disturbance immunity performance. The method introduces the compensation function observer into the LADRC and then designs the speed loop controller. Simulation results show that the CFO-LADRC-based control strategy improves control accuracy, speeds up the system response, and also reduces the difficulty of controller parameter adjustment. Compared with the traditional LADRC method, the proposed CFO-LADRC strategy exhibits more accurate disturbance observation capability and excellent disturbance rejection performance.

References

[1] Zhang E, Yu S, Wang H, et al. Overview of the Development and Application of Wind Turbine Generators[J]. Journal of Electrical Engineering, 2025, 20(1): 14-25.
[2] Qais M H, Hasanien H M, Alghuwainem S. A novel LMSRE-based adaptive PI control scheme for grid-integrated PMSG-based variable-speed wind turbine[J]. International Journal of Electrical Power & Energy Systems, 2021, 125: 106505.
[3] Jiang Q, Zeng X, Li B, et al. Time-sharing frequency coordinated control strategy for PMSG-based wind turbine[J]. IEEE Journal on Emerging and Selected Topics in Circuits and Systems, 2022, 12(1): 268-278.
[4] Thomas T, Mishra M K, Kumar C, et al. Control of a PV-wind based DC microgrid with hybrid energy storage system using Lyapunov approach and sliding mode control[J]. IEEE Transactions on Industry Applications, 2024, 60(2): 3746-3758.
[5] Lin P, Zhang S, Wu Z, et al. A linear-nonlinear switching active disturbance rejection voltage controller of PMSG[J]. IEEE Transactions on Transportation Electrification, 2022, 8(3): 3367-3378.
[6] Zhang L, Li S, Zhang Design of active disturbance rejection controller in speed loop for permanent magnet synchronous wind power generation system[J]. Control Engineering of China, 2022, 29(9): 1645-1651.
[7] Fang Y, Zeng Z, Liu Q, et al. Maximum power point tracking with nonlinear disturbance rejection control for DPMSG wind power generation system[J]. Power System Protection and Control, 2019,47(5):145-151.
[8] Li J, Zhang K, Li S, et al. Maximum power point tracking control with active disturbance rejection controller based on the best tip speed ratio[J]. Electric Machines and Control, 2015, 19(12): 94-100+106.
[9] Li S, Cao M, Li J, et al. Sensorless-based active disturbance rejection control for a wind energy conversion system with permanent magnet synchronous generator[J]. IEEE Access, 2019, 7: 122663-122674.
[10] Mo Y, Xu D, Shi H, et al. Self-correcting composite active disturbance rejection control of maximum power model for wind turbines[J]. Journal of Jiangsu University (Natural Science Edition), 2023, 44(03): 337-343.
[11] Liu Y, Zhang H, Wang M. Speed loop control of permanent magnet direct-drive wind power system based on fuzzy linear self-immunity[J]. Modern Manufacturing Engineering, 2025, (02): 144-150.
[12] Wang C, Yan J, Heng P, et al. Enhanced LADRC for permanent magnet synchronous motor with compensation function observer[J]. IEEE Journal of Emerging and Selected Topics in Power Electronics, 2023, 11(3): 3424-3434.